RSC Advances

PAPER

View Article Online
View Journal | View Issue

Cite this: *RSC Adv.*, 2025, **15**, 31019

Computational insights into phthalimide-core non-fullerene acceptors for next-generation organic solar cells

Zunaira Khan,[a] Hussain J. Alathlawi,[b] Karrar Hazim Salem,[c] Syed Muhammad Kazim Abbas Naqvi, *[de] Ines Hilali Jaghdam,[f] Mohamed S. Soliman,[g] Tamer H. A. Hasanin,[h] Sajjad Ali,[a] Haq Nawaz Bhatti*[a] and Rasheed Ahmad Khera *[a]

Traditional fullerene-based acceptors in organic solar cells (OSCs) suffer from limitations such as poor tunability, narrow absorption spectra, and limited morphological stability, restricting further improvements in device efficiency. To address these challenges, non-fullerene acceptors (NFAs) with tunable energy levels and broad optical absorption have gained increasing attention. In this study, seven novel phthalimide core-based donor–acceptor molecules (BPDM1–BPDM7) are computationally designed by modifying the terminal units of a reference molecule (BPDF). Using density functional theory (DFT) and time-dependent DFT (TD-DFT) calculations at the B3LYP/6-31G(d,p) level, photovoltaic parameters such as bandgap, frontier orbital energies, absorption maxima, light harvesting efficiency (LHE), reorganization energies (λ_e, λ_h), dipole moments, open-circuit voltages (V_{oc}), and fill factors (FF) are systematically evaluated. The designed derivatives exhibit narrow bandgap (1.84–2.18 eV) and red-shifted absorption (681–829 nm). BPDM3 shows the lowest bandgap (1.84 eV). BPDM7 achieves the highest dipole moment (3.88 D), V_{oc} (1.93 V), and FF (92.96%), while BPDM4 displays the lowest λ_e and λ_h values, indicating superior charge mobility. The reduced exciton binding energies across all derivatives suggest enhanced charge separation capabilities. These results not only provide a pathway for rational NFA design but also serve as a theoretical foundation for future experimental development of high-efficiency OSCs.

Received 25th June 2025
Accepted 14th August 2025

DOI: 10.1039/d5ra04527d

rsc.li/rsc-advances

1. Introduction

Organic solar cells (OSCs) have emerged as a favourable substitute to traditional silicon-based photovoltaics, owing to their advantages such as low manufacturing costs, mechanical flexibility, lightweight nature, and compatibility with solution-based fabrication processes.[1–4] These make the OSCs ideal candidates for energy-related applications. In the OSC structure, an active layer is constructed by an electron donor and acceptor to realize efficient exciton dissociation and charge transfer. Fullerene derivatives, especially PCBM, have been widely used as the acceptor materials because of the high electron mobility and the good energy level matching with typical donor polymers.[5,6] However, fullerene acceptors have their intrinsic limitations, including lower absorption in the visible range, unstable morphology, and high cost. In response to these shortcomings, non-fullerene acceptors (NFAs) have made substantial headway and are now the mainstream in high-efficiency OSCs.[7,8] NFAs have several merits, such as tuneable energy levels and stronger and broader absorption bands, improved morphological stability, and higher open circuit voltages (V_{oc}), which can be used to minimize energy level loss. NFAs combine structural versatility with measurable performance advantages, particularly through precise control of energy levels and broad light absorption. For example, the widely studied ITIC molecule features a LUMO of −4.00 ± 0.05 eV and a HOMO of −5.75 ± 0.10 eV, enabling efficient alignment with donor materials. Ultrawide absorption NFAs with optical gaps as low as 1.24 eV have achieved short circuit

[a]*Department of Chemistry, University of Agriculture, Faisalabad 38000, Pakistan*
[b]*Department of Physical Sciences, Physics Division, College of Science, Jazan University, P.O. Box. 114, Jazan 45142, Kingdom of Saudi Arabia*
[c]*College of Medical and Health Technologies, Al-Zahraa University for Women, Karbala, Iraq*
[d]*Faculty of Materials Science, Shenzhen MSU-BIT University, Shenzhen, 518115, China*
[e]*Platform for Applied Nanophotonics, Institute of Advanced Interdisciplinary Technology, Shenzhen MSU-BIT University, Shenzhen, 518115, China*
[f]*Department of Computer Science and Information Technology, Applied College, Princess Nourah bint Abdulrahman University, P.O. Box 84428, Riyadh 11671, Saudi Arabia*
[g]*Department of Electrical Engineering, College of Engineering, Taif University, Taif, 21944, Saudi Arabia*
[h]*Department of Chemistry, College of Science, Jouf University, P.O. Box 2014, Sakaka, Saudi Arabia*

current densities of 25.3 mA cm^2 while keeping energy losses near 0.51 eV. Likewise, fused-ring NFAs such as Y6 absorb strongly into the near-infrared (700–1000 nm), helping push single-junction efficiencies toward 19%.[9] These quantitative benchmarks illustrate how tailoring NFA properties can directly translate into higher photocurrents and improved device efficiency. In the NFAs, fused-ring electron acceptors (FREAs) have produced impressive power conversion efficiencies (PCEs) because of their rigid, planar π-conjugated backbones, enabling strong π–π stacking and efficient charge transfer.[10,11] However, FREAs suffer from the complexity of multistep synthesis, the high molecular weight, and the lack of scalability that leave outlook for their industrial use.[12,13] These problems have stimulated an increasing interest in the non-fused-ring acceptors (NFRAs) that still possess good optoelectronic properties with the advantage of easy synthesis, low cost production, higher solubility and processability.[14,15] Thus, by rational molecular design, especially by adjusting terminal acceptor groups, NFRAs can realize an optimal energy level alignment and intermolecular packing.[16] End-group engineering of NFAs among the various methods, end-group engineering represents a highly efficient and versatile method for tuning the electronic and optical properties of NFAs. Unlike core or spacer modify, it would not only allow more design flexibility, but also result in a good control of the key performance parameters.[17,18]

Prompted by the encouraging contribution of end-group engineering to the improvement of NFRA properties, we take phthalimide-core NFRA molecule, BPDF, as a reference freedom for the iteration of a structural transformation.[19] The primary goal is to enhance the optoelectronic properties of the acceptor segments and avoid crystallization of the acceptor components by engineering the end acceptor units. To achieve this goal, seven new BPDF derivatives (BPDM1–BPDM7) with different electron-withdrawing end groups were designed. These modifications included functionalizing the end groups of reference molecule R, possessing a difluorobenzothiadiazole unit and cyano (–CN) and fluoro (–F) functionalities. The alkylated compounds were then computationally examined in detail to explore the effects of end-group variation on the electronic and optical properties. Molecule R has a donor as its central unit, with acceptor groups affixed to its ends in an A–π–D–π–A configuration. To promote effective charge transfer, all the designed molecules contain spacers that connect the donor and acceptor moieties. In BPDM2, terminal units were modified with dicyano-naphthalimide groups to increase the π-conjugation as well as the electron-withdrawing character. BPDM2 retains the fluorine atoms but introduces a carbonyl-linked naphthalene unit to modulate planarity and electron affinity. BPDM3 substitutes the bridging atom with nitrogen in the benzothiadiazole framework, potentially shifting electronic distribution and ICT characteristics. BPDM4 simplifies the end group to a ketone-functionalized naphthalene without cyano groups, aiming to investigate the role of weaker acceptor strength. In BPDM5, strong electron-withdrawing ester (–$COOCH_3$) and cyano groups were incorporated. BPDM6 contains a nitro (–NO_2) and a chlorine (–Cl) group, which are anticipated to exert the strongest electron withdrawing effect and the lowest lying LUMO of the series. Finally, BPDM7 features a mixture of moderate donor–acceptor interaction and stronger dipolar character and includes methylthio (–SCH_3) and cyano groups.

In order to explore the impact of end-group variation on optoelectronic properties, all the derivatives were fully computationally characterized using Density Functional Theory (DFT)[20] and time-dependent DFT (TD-DFT).[21] Such calculations make it possible to predict quantities that are not directly measurable, these include: energy levels, absorption spectra and reorganization energies. The findings in such a theoretical study will provide useful information on the rationally design of the low cost, large scale and high performance phthalimide-based NFRA materials for future organic photovoltaic.

2. Computational methodology

All the calculations were carried out with the Gaussian 09 simulation package.[22] The molecular structures and orbitals were analysed using GaussView 6.0. To determine the most appropriate DFT method for the intended molecules, the reference molecule (R) was first optimized with four different functionals as B3LYP,[23] CAM-B3LYP,[24] MPW1PW91,[25] and WB97XD.[26] Among these functionals, the B3LYP functional yielded the best correlation with the experimentally reported absorption maximum of the reference molecule (652 nm), reported from the literature,[19] giving a theoretical value of 670 nm. Based on this result, all seven designed molecules were subsequently optimized using the B3LYP/6-31G(d,p) functional basis set.[27]

To analyse the electronic structure and density of states (DOS), PyMOlyze-1.1 [28] was employed for plotting and visualization. Additionally, key molecular properties, including the dipole moment (μ),[29] binding energies (E_b),[30] and open circuit voltage (V_{oc})[31] were computed to assess the charge distribution, interfacial compatibility, and photovoltaic potential of the designed molecules. The transition density matrix (TDM)[32] was calculated using Multiwfn software[33] to clarify the character and magnitude of charge transfer from donor to acceptor fragments. Also, the reorganization energy (λ), which is an important parameter that determines the charge mobility, was estimated for both electrons and holes.[34,35] This parameter is directly correlated with the efficiency of charge transport and was calculated according to Marcus theory.[36] The reorganization energies were obtained through the following expression:

$$\lambda_e = \left[E_\circ^- - E_-\right] + \left[E_-^\circ - E_\circ\right] \quad (1)$$

$$\lambda_h = \left[E_\circ^+ - E_+\right] + \left[E_+^\circ - E_\circ\right] \quad (2)$$

E_- is the energy of the relaxed anion and E_-° is the single point energy of the anion using the optimized geometry of the neutral. Likewise, E_+ is the total energy of the optimized cationic species, and E_+° is the single point energy of the cation on the neutral geometry. These energy values are subsequently utilized in the Marcus theory equations to calculate the reorganization electrons (λ_e) and holes (λ_h) that correlate with charge transport across the organic semiconducting materials.

3. Optoelectronic characteristics

3.1 Structural optimization

The geometry of the reference molecule (R) was optimized in solvent phase by other DFT approaches, such as B3LYP, CAM-B3LYP, WB97XD and MPW1PW91 in order to test the performance of different DFT functionals. Of these, B3LYP was found to be the most suitable functional as it provided a calculated absorption maximum of 670 nm, which is relatively close to the experimental maximum of 652 nm, as shown in **Fig. S1**. Based on this validation, the B3LYP functional was employed for the optimization of all molecules in the study. Molecule R was structurally modified by introducing different electron-accepting groups at the terminal ends, connected *via* π-spacer units. These modifications resulted in seven novel derivatives (BPDM1–BPDM7), each incorporating a unique end-group while preserving the core structure. As a result, all designed molecules follow an acceptor–spacer–donor–spacer–acceptor (A–π–D–π–A) configuration, as illustrated in Fig. 1. Both the R and all designed molecules were then optimized at the B3LYP/6-31G(d,p) level of theory to study the effect of substitution pattern on the optoelectronic properties and application in organic photovoltaic. The nitro group in BPDM6 could, at first glance, raise questions about stability. However, nitroaromatic compounds are generally quite resilient, thanks to the strong electron-withdrawing effect of the nitro group and the stabilizing influence of the aromatic ring.[37] They tend to resist both oxidative and biological degradation, and their breakdown under light is typically slow unless powerful oxidants, such as hydroxyl radicals, are present.[38,39] For this reason, under normal operating conditions and illumination, BPDM6 is expected to remain structurally stable over the device relevant lifetime.

The photoelectric characteristics are significantly influenced by bond length and dihedral angles.[40] The dihedral angles between the π bridge and acceptor parts explain the proposed molecules spatial arrangement and torsion.[41] Bond lengths and bond angles between the π-bridge and acceptor subunits were analysed from the optimized geometries of the molecules to

Table 1 Structural parameters of the R and designed molecules derived from optimized geometries

Molecules	Interatomic distance, I_{C-C} (Å)	Torsional angle, θ (°)	MPP (Å)	SDP (Å)
R	1.42	0.13	1.11	4.94
BPDM1	1.42	0.11	1.29	5.24
BPDM2	1.42	0.13	1.22	5.02
BPDM3	1.44	0.03	0.90	4.39
BPDM4	1.43	0.58	0.87	4.33
BPDM5	1.41	0.03	1.37	6.82
BPDM6	1.42	2.79	1.25	6.02
BPDM7	1.42	0.03	1.31	6.64

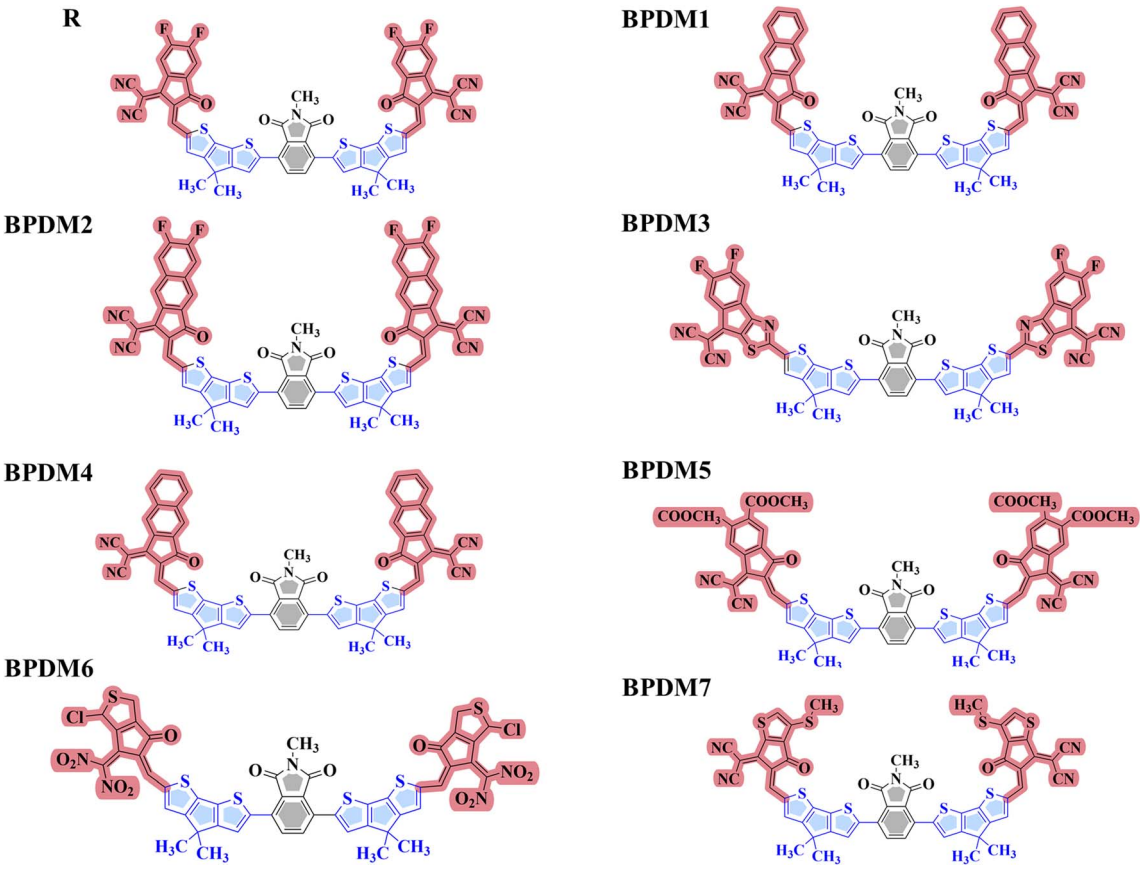

Fig. 1 The representation of geometry of R and designed molecules (BPDM1–BPDM7) using B3LYP/6-31G(d,p) level of theory.

gain insight into their structural organization and electronic interactions. The corresponding values are summarized in Table 1. In addition, the bond angle between the spacer and acceptor units is key to determining the molecule planarity. A lower dihedral (torsional) angle generally corresponds to a more planar conformation, which facilitates better π-electron delocalization and enhances conjugation. All the designed molecules exhibit torsional angles in the range of 0.03° to 2.79°, indicating a high degree of planarity. The lowest torsional angle is observed in BPDM5, with a value of 0.02°, suggesting that it possesses the most planar configuration among the series. The interatomic distances between the π-bridge and terminal acceptor groups range from 1.42 to 1.44 Å, which lies between the typical C–C single bond (1.54 Å) and C=C double bond (1.34 Å) lengths. This intermediate bond length strongly indicates the presence of delocalized π-conjugation throughout the molecular backbone. These torsional angles and interatomic distances are illustrated in **Fig. S2**.

Molecular planarity plays a critical role in governing the optoelectronic performance of organic semiconductors. In this study, the Molecular Planarity Parameter (MPP) and the Span of Deviation from the Plane (SDP) were employed to quantitatively evaluate the geometric planarity of the reference and designed molecules. MPPs were analysed with Multiwfn 3.8, and molecular visualizations were created with VMD 1.9.3.[42] A higher MPP value corresponds to a larger deviation from planarity, which means the flatter configuration is favourable for the effective π–π stacking and promotes charge transport in OSCs.[43] SDP quantifies the highest vertical range of atomic displacements to the fitting plane and describes the amount of local distortion. MPP and SDP in combination, therefore, provide a full assessment of molecular coplanarity, a critical determinant of the intermolecular interactions, charge delocalisation, and device performance. The lower MPP and SDP values, the better the orbital overlap and the charge carrier mobility, and higher MPP and SDP values are indicative of turning conformations, which spoil the π-conjugation and suppression of photovoltaic efficiency.[44,45] The calculated MPP values for R and designed molecules are 1.11, 1.29, 1.22, 0.90, 0.87, 1.37, 1.25, and 1.31 Å, respectively. BPDM4 shows the lowest MPP value, indicating superior structural planarity. In contrast, BPDM5 shows the highest MPP value, suggesting greater torsion within its molecular framework. Corresponding SDP values are 4.94, 5.24, 5.02, 4.39, 4.33, 6.82, 6.02, and 6.64 Å, further confirming the enhanced planarity of BPDM4 relative to the other derivatives. These geometrical parameters are tabulated in Table 1 and illustrated in **Fig. S3**.

3.2 Optical absorption characteristics

The optical characteristics of molecules are crucial in determining the photovoltaic performance in OSCs.[46] The excited state parameters have gained acceptance in studying the mechanisms of underlying photocurrent generation and their relationship to spectral features. The R and designed molecules absorption spectra are computed by B3LYP/6-31G(d,p). The calculated oscillator strength (*f*), dipole moment (D), and maximum absorption (λ_{max}) of R and designed molecules in the gaseous phase and solvent are tabulated in **Table S1** and **Table S2** respectively. The value of λ_{max} is significantly influenced by the modification of R with a new acceptor at the terminal of the molecule. Electron attracting effect of the terminal acceptor is elevated which elevates the λ_{max} values of these molecules and in turn, it decreases the bandgap (E_g) by affecting HOMO and LUMO values. So, there is an inverse relationship between λ_{max} and E_g and the study of literature also makes clear that the low E_g causes the absorption spectra to redshift and the same trend results have shown.[47]

The λ_{max} values for R and the designed molecules fall within the range of 629–758. All compounds have shown redshift absorption following R. The strongest redshift is shown in BPDM3 it has the highest value of 758 nm means maximum wavelength is highly influenced by the introduction of terminal recipient group. The λ_{max} values is in the order of BPDM3 > BPDM4 > BPDM6 > BPDM2 > BPDM1 > BPDM7 > BPDM5 > R. The minimum value of λ_{max} is of molecule BPDM5 which is 639 nm. In the presence of solvent (chloroform), values of λ_{max} of all the designed molecules exceed the R. It is estimated that BPDM3 has the highest λ_{max} value then all other designed molecules because of n–π* transitions and electron-withdrawing –CN group. Furthermore, all the designed molecules exhibit broader absorption spectra than the R in gas phase and solvent. All designed molecules exhibit significant absorption in both the visible and near infrared regions, indicating their strong potential for efficient photon harvesting in OSCs applications. The results demonstrate that designed molecules possess enhanced absorbance compared to the R, suggesting their suitability as promising active materials in high performance OSCs. The simulated absorption spectras of BPDM1–BPDM7 are illustrated in Fig. 2.

3.3 Oscillator strength and excitation energy

The transition probabilities are commonly referred to as oscillation strength (*f*) and the energy required for this transition is known as excitation energy (E_X).[48] It forecasts that the effective intermolecular charge transfer (ICT) will display significant oscillations at low excitation energy and a wider absorption alongside a greater molar absorption coefficient.[49] The maximum value of molar absorption coefficient of the designed molecules is calculated up to 10 excited states to get a deeper understanding of optical properties. However, the excited state

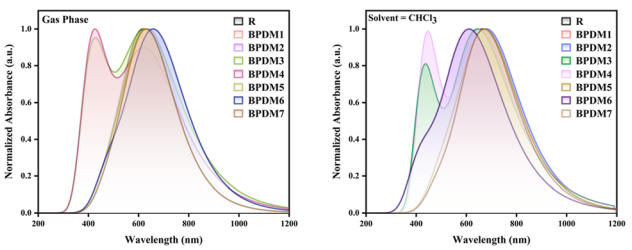

Fig. 2 Graphical representation of UV-Vis absorption for R and designed molecules (M1–M7), in gas phase as well as in solvent.

S_1 actively contributed to the HOMO–LUMO values with notable oscillator strength. The function of f of molecules is considerable in finding the photovoltaic ability. Elevation in f values increases the transition of electrons over the flow of photons.[50] The f value of the R is 2.78 in the gas phase and 3.07 in the solvent phase. The detailed f values of all designed molecules in both phases are provided in **Table S1** (gas phase) and **Table S2** (solvent phase). Among the designed derivatives, BPDM2 exhibits the highest f, with values of 3.38 in the solvent and 3.04 in the gas phase. All of the designed molecules, except BPDM3 and BPDM4, demonstrate notably high f values. A higher oscillator strength means the material interacts more strongly with incoming light, making photon absorption more likely. In NFAs, this strong light absorption across the visible to near-infrared range produces more excitons, which, if they are efficiently split and moved through the device, can boost the photocurrent and increase the short-circuit current density. This suggests that the designed molecules possess strong photon-harvesting capabilities, which are critical for facilitating efficient photoexcitation in OSCs.

The E_X represents the energy required for the transition of an electron from the HOMO to the LUMO. A lower E_X value facilitates easier electron excitation from the ground to the excited state, thereby enhancing charge transfer efficiency. Notably, excitation energy and charge transfer exhibit an inverse correlation, lower excitation energies typically correspond to more effective ICT. For R, the E_X is calculated to be 1.96 eV in the gas phase and 1.84 eV in the solvent phase. E_X values for the designed molecules were calculated in both the gas and solvent (chloroform) phases to evaluate their optical properties relative to the reference. A comprehensive summary of the E_X values for all designed molecules in both gas and solvent phases are provided in **Tables S1** and **S2**. Among all derivatives, BPDM3 exhibits the lowest E_X in both environments, which can be attributed to its enhanced n–π* transition character. In general, the reduced energy gaps between the n and π* orbitals observed across the designed molecules facilitate easier electronic transitions upon light absorption. Furthermore, their consistently low E_g, along with the presence of strong electron-withdrawing groups such as –CN, $-NO_2$, and –Cl at the terminal acceptor positions, contribute to enhanced ICT. The E_X values of all the designed molecules are lower than that of the R in both gas and solvent phases. These characteristics collectively indicate that the designed molecules possess excellent potential as efficient photoactive materials for application in OSCs.

3.4 The frontier molecular orbitals (FMOs)

Molecular orbitals are fundamental descriptors in quantum chemistry used to examine charge transfer, molecular interactions, and electronic distribution, particularly in the design of organic optoelectronic materials. In the context of OSCs, FMOs are directly related to light absorption, photoexcitation, and the efficiency of charge transport. Chemical softness and hardness are also important indicators of molecular reactivity and stability.[51] A smaller E_g, which corresponds to higher softness and lower hardness, facilitates electronic transitions and supports efficient photon absorption and electron acceptance.[52] Upon photoexcitation, electrons shift from the HOMO to the LUMO, transitioning from the ground state to the excited state. Usually, a smaller E_g enhances ICT.[53] Moreover, the presence of a greater electron density in the HOMO on the π-bridge and LUMO localization on the acceptor units promotes directional charge transfer toward the terminal acceptors upon excitation. The HOMO–LUMO energy levels and corresponding E_g values for the R and the designed derivatives were calculated to assess their electronic structures. These values are summarized in **Table S3**.

The lowered LUMO levels in the designed molecules, especially those with strong electron-withdrawing groups at the terminal acceptors, result in narrower E_g relative to the R. Consequently, all the designed molecules exhibit improved charge transfer capability and enhanced optoelectronic properties. The calculated E_g values in ascending order are: BPDM3 (1.85), BPDM4 (1.88), BPDM6 (2.07), BPDM2 (2.13), BPDM1 (2.15), BPDM7 (2.17), BPDM5 (2.18), and R (2.20). The FMO distributions of the R and designed molecules are depicted in Fig. 3, illustrating that in the ground state, the HOMO is primarily delocalized over the donor core and π-bridge, while in the excited state, and the LUMO becomes more localized on the terminal acceptor units. This spatial separation of HOMO and LUMO confirms efficient ICT upon excitation, which is a key feature for high-performance OSCs. The R exhibits higher E_g compared to the BPDM1–BPDM7; this can be attributed to the absence of a strongly electron-withdrawing end-capped acceptor group. Consequently, it encounters more challenges in promoting the excitation of electrons from the HOMO to the LUMO. Among the designed molecules, BPDM3 incorporates a highly electron-withdrawing acceptor unit, which enhances ICT and results in the lowest E_g value within the series. The reduced E_g is a key parameter that supports its potential as an efficient active material in OSCs.

3.5 Density of state (DOS) analysis

The study of the Density of States (DOS) is helpful to analyse the distribution of energy levels in the frontier molecular orbitals (FMOs). It provides useful information about electronic transitions and absorption features related to different moieties of the molecule, that is, donor core, π-bridge, and terminal acceptor group. In order to access the separate contributions to the processes of each molecular fragment, three distinct molecular subunits were considered: donor core, π-bridge and terminal acceptor. From the DOS profiles, it is obvious that how the contribution to HOMO and LUMO energy levels for each fragment is. For the R and designed molecules, the HOMO were 9.5–10.5% and the LUMO were 3.0–9.6% donor core contributed. The π-bridge contributed 60.8% to 63.5% to the HOMO and 15.6% to 38.5% to the LUMO. The acceptor units contributed 26.5% to 29.5% to the HOMO and 51.9% to 81.4% to the LUMO. These values are summarized in **Table S4**.

The data reveal that the LUMO is predominantly localized on the acceptor fragments across all designed molecules, significantly more than on the donor cores. This strong LUMO

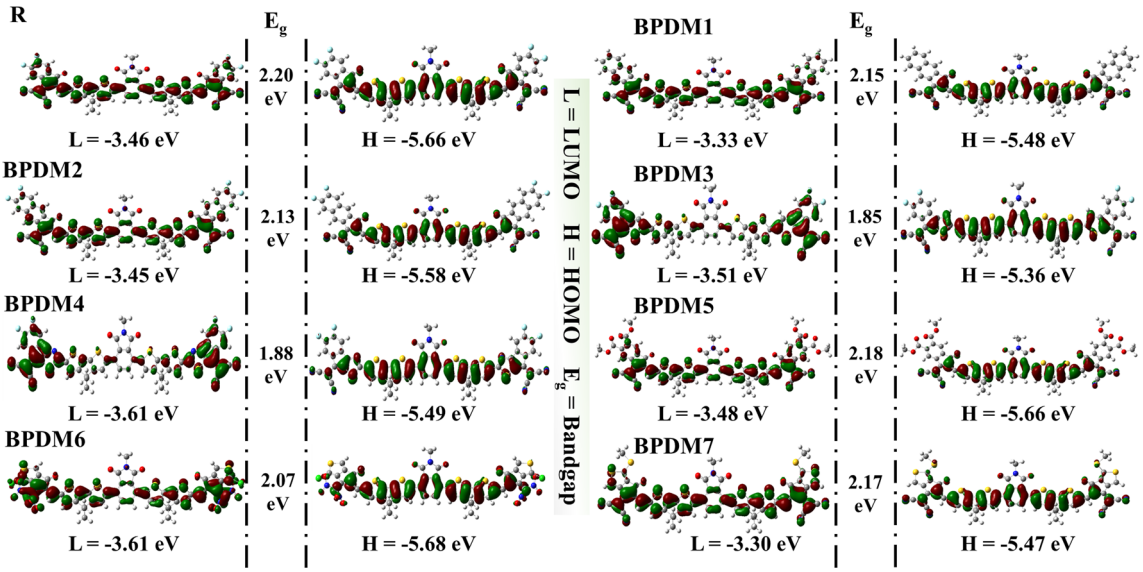

Fig. 3 FMOs diagram of R and designed molecules (BPDM1–BPDM7).

contribution from the terminal acceptors confirms their role in facilitating ICT. The enhanced electron-withdrawing capacity of the terminal groups in BPDM1–BPDM7, compared to the fluorinated end group of the reference molecule, leads to a notable reduction in E_g, as observed in Fig. 4. In particular, the incorporation of strongly electron-withdrawing substituents and extended conjugation in the modified molecules enhances their ability to draw electron density, thereby improving charge separation and transport. The DOS analysis validates the design strategy of strengthening the acceptor groups in the newly developed molecules. The increased LUMO contribution by the terminal acceptors and the resulting narrowing of the E_g are critical factors in improving the optoelectronic properties and photovoltaic performance of these materials.

3.6 Molecular electrostatic potential (MEP)

The molecular electrostatic potential (MEP) analysis is a valuable approach for visualizing the electron density distribution across a molecule and identifying regions of electrophilic and nucleophilic reactivity. MEP maps provide insight into the nature of charge separation and intramolecular interactions, which are critical for evaluating the optoelectronic behaviour of organic semiconductors. From the perspective of electronic

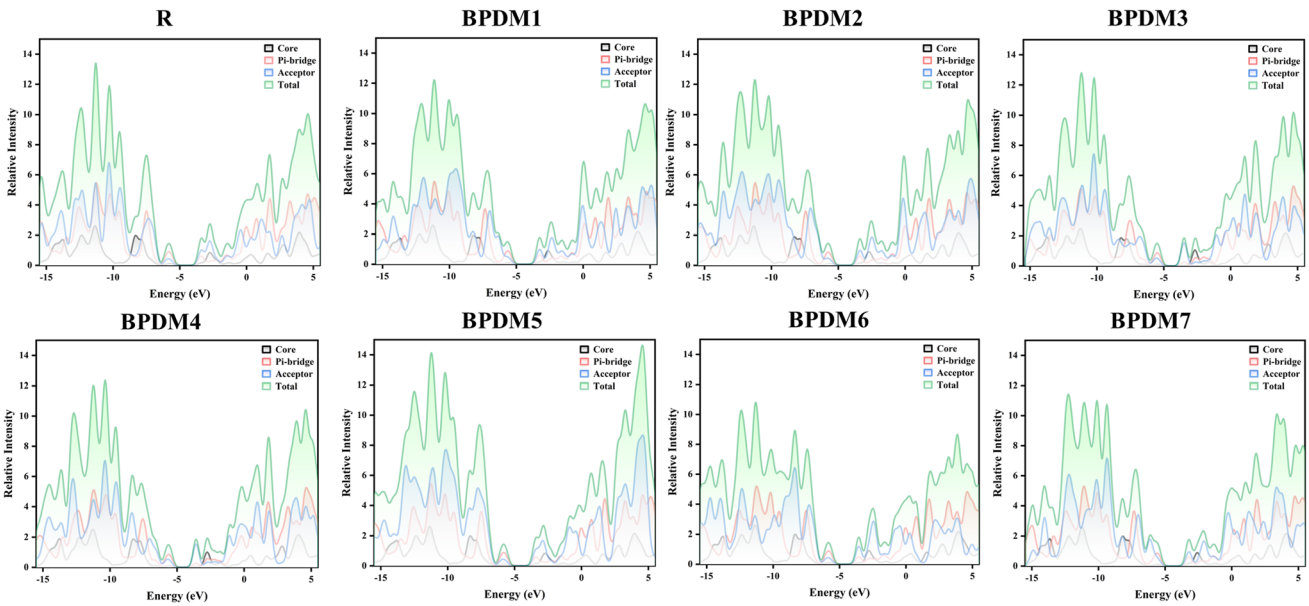

Fig. 4 DOS spectra of the R and designed molecules (BPDM1–BPDM7), showing the contributions of donor core, π-bridge, and terminal acceptor to the HOMO and LUMO regions.

properties in OSCs, MEP analysis assists in understanding the directionality and efficiency of charge transfer pathways within donor–acceptor systems. The electrostatic potential on the molecular surface is color-coded to reflect the local charge environment. Typically, red and yellow regions represent negative electrostatic potential and are associated with electron-rich (acceptor) sites, whereas blue regions indicate positive electrostatic potential, corresponding to electron-deficient (donor) areas. Green regions represent areas of neutral potential. The electrostatic potential generally follows the gradient: red < yellow < green < cyan < blue, moving from the most negative to the most positive potential.[54]

Fig. 5 displays the MEP surfaces of the R and the designed molecules. Within all molecules, the central donor cores are mainly marked by blue regions, whereas the terminal acceptor units feature red, yellow, and light green areas. This pattern reflects a directional charge separation from the electron-donating core to the electron-withdrawing ends, supporting efficient ICT upon excitation. Among all derivatives, BPDM6 displays the most pronounced red zones at the terminal ends, which is attributed to the strong electron-withdrawing nature of the oxygen and nitrogen atoms present in its acceptor groups. These highly electronegative atoms pull electron density toward the acceptor, enhancing charge separation and improving charge mobility. This observation further supports the role of structural design in modulating electronic properties. MEP analysis confirms that all designed molecules exhibit effective charge separation and favourable electron density distribution, which are essential characteristics for high performance photoactive materials in OSCs.

3.7 Exciton binding energy (E_b)

Exciton binding energy (E_b) is an essential statistical instrument for the estimation of photovoltaic parameters and the operating efficiency of OSCs. Exciton dissociation of constrained electron–hole pairs is analysed by using a coulombic interaction. After excitation, the least energy is needed to separate the charges and allow them to move toward their compatible electrodes. This energy is the excitation binding energy. Reduced binding energy highlights the weakened coulombic interactions, facilitating the straightforward dissociation of excitons, which in turn promotes easier charge flow. So, the introduction of a stronger acceptor in R causes weaker coulombic forces thus it generates free electrons and hole moieties and lowers the E_b needed for simpler dissociation.[55] The E_b values for all the designed molecules can be found in **Tables S1** and **S2** which shows that there is a clear drop in the binding energies of the reported molecules which suggests that electrons and holes can separate effortlessly and ultimately increase in charge mobility. BPDM1 has a significant electron-withdrawing group that lowers the exciton binding energy so, this is a good fit for novel OSCs manufacturing.

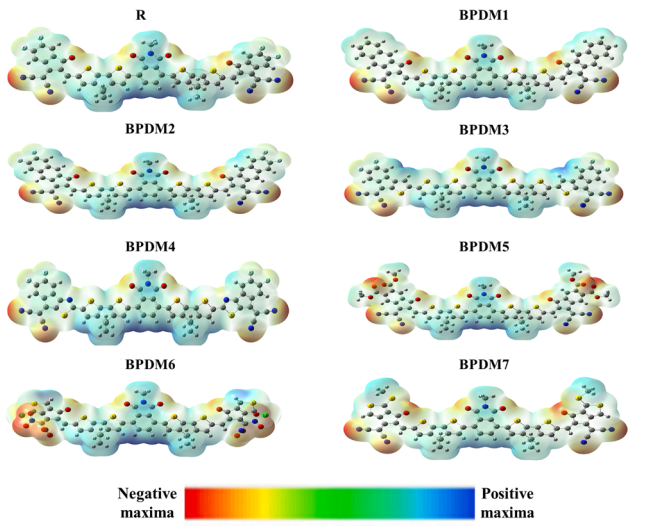

Fig. 5 MEP surfaces of the R and designed molecules (BPDM1–BPDM7), highlighting regions of electron density distribution.

3.8 Transition density matrix analysis

Transition Density Matrix (TDM) analysis offers a detailed perspective on the excited-state dynamics of molecules by illustrating how electronic charge is redistributed upon photoexcitation. This method sheds light on the spatial separation between electron and hole populations, providing valuable information about ICT efficiency and the extent of electronic delocalization. In this study, TDM analysis was applied to both the R and the designed derivatives to explore the direction and magnitude of charge movement following excitation. Hydrogen atoms were excluded from the analysis due to their negligible contribution to electronic transitions. The TDM visualizations, shown in **Fig. S3**, represent excitation characteristics using a colour mapped matrix where atomic indices (excluding hydrogens) are plotted on both axes. Colour intensity reflects the degree of electron–hole correlation. Red zones signify high electron density accumulation; blue zones indicate minimal activity, and intermediate shades represent transitional behaviour. Diagonal elements highlight localized excitations, while bright regions off the diagonal are indicative of charge movement between distant segments, pointing to effective long range ICT.

All designed molecules demonstrate consistent charge migration from the donor segment to the terminal acceptor, which is indicative of efficient charge delocalization. Particularly, BPDM6 and BPDM7 show distinct off-diagonal hotspots, suggesting more pronounced ICT behaviour than the R. These patterns reflect favourable electronic communication between molecular subunits and a design conducive to enhanced charge separation, key for improving OSC performance. To complement the visual data, interaction coefficients were extracted from the TDM matrices to quantify electron–hole coupling strength. Lower values of this parameter imply weaker electrostatic binding, supporting improved charge dissociation and transport properties. The consistently reduced interaction coefficients observed in the newly developed derivatives underscore their potential as high efficiency photoactive materials in organic photovoltaic devices.

3.9 Dipole moment (D)

The dipole moment (D) is a key parameter that reflects the degree of charge separation within a molecule and plays a vital role in determining molecular polarity, solubility, and charge transport behaviour. In the context of OSCs, efficient separation and transport of charges between donor and acceptor units significantly impact device performance. A larger dipole moment often correlates with improved solubility in polar organic solvents (*e.g.*, chloroform), better thin-film formation, and enhanced charge mobility, all of which contribute to superior photovoltaic efficiency.[56] In this study, the dipole moments of the R and all designed derivatives were calculated using the B3LYP/6-31G(d,p) level of theory. The computed values, summarized in **Tables S1** and **S2**, reveal that BPDM7 exhibits the highest dipole moment, with values of 3.88 D in the gas phase and 3.62 D in the solvent phase. These elevated values suggest a strong molecular polarity, indicating excellent solubility in common processing solvents and suitability for the formation of uniform, stable active layers. Furthermore, a higher dipole moment can enhance intermolecular interactions, promote better molecular packing, and facilitate ICT by encouraging self-assembly and crystallinity. These features collectively lead to superior hole and electron mobilities, well matched donor–acceptor architecture, and an increased fill factor, which also affords a higher device performance. The high dipole moment demonstrated by BPDM7 highlights its promise as a scale-up and efficient photoactive material for next-generation OSCs.

3.10 Light harvesting efficiency (LHE)

LHE, as an important parameter, represents a molecule performance to absorb the incident photons and generate excitons, thereby affecting the J_{sc} and PCE of OSCs. LHE is also well connected with the oscillator strength (f) of electronic transitions. Higher f generally leads to stronger absorption, stronger exciton generation, and therefore to a larger J_{sc}. LHE describes how effectively the active layer absorbs incoming photons at each wavelength. Since photocurrent generation begins with photon absorption, a higher LHE generally supports a higher J_{sc}, provided that subsequent processes such as exciton diffusion, charge separation, and charge collection are efficient. In essence, LHE sets the upper limit for the fraction of the solar spectrum that can be converted into current.[57] J_{sc} represents the integrated contribution of all absorbed photons across the spectrum; however, factors such as charge recombination or poor transport can still reduce it. This relationship between optical absorption and photocurrent is well established in organic photovoltaic research, where improved light absorption often directly enhances current output. In this work, the LHE of R and its seven designed derivatives are calculated, which are shown in **Tables S1** and **S2**. Of all the series, BPDM1 and BPDM2 possess the largest LHE values, which are indicative of better photon absorption. These results suggest their very promising application as high efficiency photoactive materials for OSCs based on the effective absorption ability toward incident light.

3.11 Global reactivity descriptors

From the energy of the frontier molecular orbital, the global reactivity descriptors could be used to calculate the chemical reactivity and kinetic stability of the organic semiconductor molecules. These parameters (ionization potential (IP), electron affinity (EA), chemical hardness (η), and global softness (S)), which can be directly computed by HOMO and LUMO energy levels, can be treated as one of the criteria for determining a good molecular candidate. In general, molecules with a smaller E_g are chemically soft and more reactive, whereas those with a larger E_g are harder and more stable. In the case of OSCs, higher molecular S and reactivity are beneficial for ICT and exciton dissociation and thus for the device performance. The IP is the energy needed to liberate an electron from the HOMO, while the EA is the energy released upon including an electron into the LUMO. These characteristics are critical in understanding the charge injection and transport properties of active layer materials. The computed IP and EA values of the R and all the designed derivatives are presented in **Table S5**, which could help to grasp the electronic reactivity of these derivatives and the compatibility for the use of OSC. The IP values follow the trend: BPDM6 > R = BPDM5 > BPDM2 > BPDM4 > BPDM1 > BPDM7 > BPDM3, whereas the EA values are ordered as: BPDM4 = BPDM6 > BPDM3 > BPDM5 > R > BPDM2 > BPDM1 > BPDM7.

The designed derivatives BPDM3 and BPDM4 exhibit relatively greater IP and EA values that indicate the favourable electron-accepting property and better charge accommodation. Apart from IP and EA, the η and S are also useful for determining the structure-molecular stability, and polarizability. Higher η values correspond to chemically less reactive and structurally more stable molecules, while those with larger S values are more reactive and are favourable for the mediation of dynamic charge-transfer processes. In OSC, such reactivity is desirable to drive efficient ICT and to enhance device performance. As such, molecules with narrow E_g tend to display reduced kinetic stability but enhanced reactivity, which is desirable for active layers in OSCs. The calculated η and S values for the R and designed molecules are presented in **Table S5**.

3.12 Reorganization energy (λ)

Reorganization energy (λ) is a key parameter in the design and evaluation of high performance materials for OSCs. It is closely associated with the charge transfer rate and, therefore, significantly impacts the overall efficiency of OSCs. The relationship between reorganization energy and charge mobility is inverse; a lower λ typically facilitates faster charge transport, which is essential for efficient device operation. λ consists of two components referred to as internal reorganization energy (λ_{int}), which includes λ_h (for hole transport) and λ_e (for electron transport), and external reorganization energy (λ_{ext}). The λ_{ext} accounts for the influence of the surrounding medium, and the internal component reflects the structural reconfiguration within the molecule as it transitions between neutral and charged states. Given the focus on isolated molecular systems, only λ_{int} is considered in this study.

Equations based on Marcus theory can be used to determine the internal component. Marcus theory establishes that the rate of charge transfer increases with decreasing λ and reaches its maximum when the driving force is equal to λ. This theoretical framework is instrumental in linking molecular structure to charge transport efficiency in organic semiconductors. According to Marcus theory, lower reorganization energy values correlate with enhanced charge carrier mobility, which is essential for obtaining high power conversion efficiencies in OSCs. Reorganization energy reflects the structural adjustments that occur upon oxidation or reduction: the geometry of the anionic state is associated with λ_e, while that of the cationic state pertains to λ_h. Accordingly, λ_e and λ_h are the main descriptors of charge transport behaviour between the donor–acceptor moieties in a molecule. Both λ_e and λ_h values are tabulated in **Table S6**, for the R and the designed derivatives. The majority of the new compounds have smaller λ_e than the R, except BPDM2 and BPDM6. This tendency implies that most modified structures are with the better electron mobility and is structurally preferred for encouraging charge transfer in OSC applications. The results demonstrate the importance of molecular design in the fine tuning of reorganization energies for improved photovoltaic performance.

4. Photovoltaic performance parameters

4.1 Open circuit voltage (V_{oc})

The open circuit voltage (V_{oc}), a key photovoltaic parameter, signifies the maximum voltage a solar cell can generate under illumination without any external current being drawn. It is also a symbolic measure of the energy level alignment of donor and acceptor materials and plays an important role in the overall PCE of OSCs. This V_{oc} is influenced by factors such as temperature and light intensity, the architecture of the device as well as, the energies of the FMOs of the donor and the acceptor. The energy offset between the HOMO of the donor and LUMO of the acceptor is one of these main contributions, which limits the possible photovoltage and charge separation efficiency of the active layer. A greater difference between these energy levels generally results in a higher V_{oc}, provided that it does not hinder efficient charge separation or increase energy loss.[58]

In this study, PM6 is used, with experimentally reported HOMO and LUMO values of −5.52 eV and −3.64 eV, respectively.[59] The designed molecules act as donor materials. The theoretical V_{oc} values were calculated using the following equation:

$$V_{oc} = \left(\frac{\left|E^{D}_{HOMO}\right| - \left|E^{A}_{LUMO}\right|}{e} \right) \quad (3)$$

Energies are denoted by E, the charge on the discrete molecule is indicated by e, and 0.3 eV represents energy losses linked to non-radiative recombination, interfacial energy barriers, and the formation of charge transfer states.[60] The V_{oc} value calculated for the R is 1.76 V. **Table S7** contains the calculated V_{oc} values of the designed molecules when combined with PM6. The order of V_{oc} values follows the trend: BPDM7 > BPDM1 > BPDM2 > R > BPDM5 > BPDM3 > BPDM4 = BPDM6. Among the derivatives, BPDM7 exhibits the highest V_{oc} of 1.93 V. A larger energy offset between these levels is favourable for achieving high V_{oc}. Conversely, molecules such as BPDM4 and BPDM6 show relatively lower V_{oc} values, likely due to their comparatively higher. Even though BPDM6 contains a nitro ($-NO_2$) group, its arrangement within a stable π-conjugated donor–acceptor structure is anticipated to encourage electronic delocalization and reduce possible reactivity. π-conjugated acceptors with a nitro group that are similar to those described in previous studies have demonstrated satisfactory stability throughout the process of producing and using OSCs, especially when they are electronically linked to the core and reinforced by steric shielding.[61,62] This structural rationale implies that BPDM6 possess adequate chemical stability for practical device applications. Too large E_g may reduce overlap and hinder efficient charge generation. The observed V_{oc} values suggest that designed molecules maintain a positive energy alignment with PM6, and particularly BPDM7 offers the most promising energy configuration for achieving high efficiency OSCs.

4.2 Fill factor (FF)

Fill factor directly impacts the overall power conversion efficiency (PCE) of OSCs. It reflects the extent to which a device approaches its maximum power output and is influenced by the quality of the donor–acceptor interface, internal resistance, charge carrier mobility, and recombination dynamics. A higher FF indicates more efficient extraction of photogenerated charge carriers and minimal losses in charge transport. It also strongly dependent on the V_{oc}, as it correlates with the built-in potential of the active layer and the capacity to sustain photogenerated charge separation under operational conditions.[63,64] FF was estimated using a semi-empirical relationship derived from the normalized open-circuit voltage:

$$FF = \frac{\frac{eV_{oc}}{k_B T} - \ln\left(\frac{eV_{oc}}{k_B T} + 0.72\right)}{\frac{eV_{oc}}{k_B T} + 1} \quad (4)$$

Here, V_{oc}, K_B, T and e are the open circuit voltage, Boltzmann constant, temperature at 300 K and the elementary charge of a molecule. The calculated FF values for R and designed molecules were listed in **Table S7**. Among the studied molecules, BPDM7 exhibits the highest FF values, indicating reduced recombination losses and efficient carrier collection. These properties make them particularly compatible for implementation in high efficiency OSC devices.

4.3 Power conversion efficiency (PCE)

Power conversion efficiency (PCE) is the most critical figure of merit for evaluating the performance of OSCs. It reflects the proportion of incident solar energy that can be converted into usable electrical energy and is determined by the combined

effects of V_{oc},J_{sc}, and FF.[65] PCE is calculated using the following equation:

$$\mathrm{PCE} = \frac{V_{oc} J_{sc} \times \mathrm{FF}}{P_{in}} \quad (5)$$

J_{sc} denotes the short circuit current density, is the open-circuit voltage, FF is the fill factor, and P_{in} represents the power of the incident light, typically considered as 100 mW cm^{-2}. Given the observed increases in V_{oc} and FF for designed molecules, their overall photovoltaic performance is expected to exceed that of the R. Based on the combined analysis of electronic structure, optical absorption, charge transport parameters, and energy loss, the designed molecules show strong potential for achieving improved PCE. The calculated PCE values for all designed molecules are summarized in **Table S7**. The calculated PCE trend among the studied molecules follows the order: BPDM7 > BPDM1 > BPDM2 = R > BPDM5 > BPDM3 > BPDM4 = BPDM6. These findings support the viability of the proposed donor structures as promising candidates for high efficiency and commercially viable OSCs. Given the observed increases in V_{oc} and FF, the designed molecules are predicted to outperform the reference, with PCE values (**Table S7**) following the trend: BPDM7 > BPDM1 > BPDM2 = R > BPDM5 > BPDM3 > BPDM4 = BPDM6. These represent theoretical upper limits based on assumed J_{sc} values. Although this study is computational, the donor–acceptor frameworks are similar to experimentally reported molecular designs,[19,66] and the predicted properties fall within ranges achieved by high-efficiency OSC materials, indicating feasibility for synthesis and device fabrication.[67,68]

5. Conclusions

In this study, seven novel A–π–D–π–A phthalimide-based non-fullerene acceptor molecules were designed *via* terminal group engineering and evaluated through quantum chemical simulations to examine their optoelectronic and charge transport properties for use in OSCs. All designed molecules exhibited reduced narrower E_g (1.85–2.18 eV), redshifted absorption spectra, and improved frontier orbital alignment. DOS and TDM analyses confirmed pronounced ICT and effective electron density redistribution, supporting efficient charge separation. Among the designed molecules, BPDM1, BPDM2, and BPDM7 demonstrated the most promising photovoltaic profiles when paired with PM6 as the donor, combining optimal V_{oc}, high FF, and low reorganization energies conducive to enhanced electron mobility. These results highlight BPDM1, BPDM2, and BPDM7 as strong candidates for next generation high performance OSCs. Furthermore, the insights gained from this work provide molecular-level design guidelines for developing efficient non-fullerene acceptors with superior optoelectronic properties.

Author contributions

H. N. Bhatti and R. A. Khera conceived and designed the study; Z. Khan, H. J. Alathlawi, K. H. Salem, and S. M. K. A. Naqvi carried out the computational modeling, simulations, and figure preparation; I. H. Jaghdam, and M. S. Soliman contributed to data analysis and interpretation; T. H. A. Hasanin, S. Ali, and Z. Khan participated in writing and editing the manuscript; S. Manzoor revised the manuscript.

Conflicts of interest

No potential conflicts of interest have been disclosed by the authors.

Data availability

Data for this article obtained from density functional theory (DFT) and time-dependent density functional theory (TD-DFT) methods, including geometry optimisation, density of states (DOS) analysis, natural transition orbitals (NTO), transition density matrix (TDM) calculations, and total energy computations, are available at Mendeley data at DOI: **https://doi.org/10.17632/rxfr3b5wbz.1**. Further details related to data are available in the SI. See DOI: **https://doi.org/10.1039/d5ra04527d**.

Acknowledgements

The authors extend their appreciation to the Princess Nourah bint Abdulrahman University Researchers Supporting Project number (PNURSP2025R845), Princess Nourah bint Abdulrahman University, Riyadh, Saudi Arabia.

References

1 Q. Dong, M. Chen, Y. Liu, F. T. Eickemeyer, W. Zhao, Z. Dai, Y. Yin, C. Jiang, J. Feng, S. Jin, *et al.*, Flexible Perovskite Solar Cells with Simultaneously Improved Efficiency, Operational Stability, and Mechanical Reliability, *Joule*, 2021, **5**(6), 1587–1601.
2 M. Riede, D. Spoltore and K. Leo, Organic Solar Cells—The Path to Commercial Success, *Adv. Energy Mater.*, 2021, **11**(1), 2002653.
3 D. Luo, W. Jang, D. D. Babu, M. S. Kim, D. H. Wang and A. K. K. Kyaw, Recent Progress in Organic Solar Cells Based on Non-Fullerene Acceptors: Materials to Devices, *J. Mater. Chem. A*, 2022, **10**(7), 3255–3295.
4 Y. Cui, H. Yao, J. Zhang, K. Xian, T. Zhang, L. Hong, Y. Wang, Y. Xu, K. Ma, C. An, *et al.*, Single-Junction Organic Photovoltaic Cells with Approaching 18% Efficiency, *Adv. Mater.*, 2020, **32**, 1908205.
5 C. Chen, X. Wang, Z. Li, X. Du, Z. Shao, X. Sun, D. Liu, C. Gao, L. Hao, Q. Zhao, *et al.*, Polyacrylonitrile-Coordinated Perovskite Solar Cell with Open-Circuit Voltage Exceeding 1.23 V, *Angew. Chem., Int. Ed.*, 2022, **61**, e202113932.
6 S. M. Kazim Abbas Naqvi, F. Abbas, S. Bibi, M. K. Shehzad, N. Alhokbany, Y. Zhu, H. Long, R. B. Vasiliev, Z. Nazir and S. Chang, Theoretical Investigation of Benzodithiophene-Based Donor Molecules in Organic Solar Cells: From Structural Optimization to Performance Metrics, *RSC Adv.*, 2024, **14**(41), 29942–29954.

7 C. Li, J. Zhou, J. Song, J. Xu, H. Zhang, X. Zhang, J. Guo, L. Zhu, D. Wei, G. Han, *et al.*, Non-Fullerene Acceptors with Branched Side Chains and Improved Molecular Packing to Exceed 18% Efficiency in Organic Solar Cells, *Nat. Energy*, 2021, **6**, 605–613.
8 J. Zhang, H. S. Tan, X. Guo, A. Facchetti and H. Yan, Material Insights and Challenges for Non-Fullerene Organic Solar Cells Based on Small Molecular Acceptors, *Nat. Energy*, 2018, **3**(9), 720–731.
9 C. Yan, S. Barlow, Z. Wang, H. Yan, A. K. Y. Jen, S. R. Marder and X. Zhan, Non-Fullerene Acceptors for Organic Solar Cells, *Nat. Rev. Mater.*, 2018, **3**, 18003.
10 J. Wang, P. Xue, Y. Jiang, Y. Huo and X. Zhan, The Principles, Design and Applications of Fused-Ring Electron Acceptors, *Nat. Rev. Chem.*, 2022, **6**, 614–634.
11 C. Zhang, Y. Zhang, L. Wang, H. Wu, B. Wu, Z. Tang, W. Ma, Z. Luo, C. Li, Z. Bo, *et al.*, High-Performance Non-Fullerene Organic Solar Cells Enabled by Noncovalent Conformational Locks and Side-Chain Engineering, *Chem. Eng. J.*, 2022, **446**, 137206.
12 B. Kan, Y. Kan, L. Zuo, X. Shi and K. Gao, Recent Progress on All-small Molecule Organic Solar Cells Using Small-molecule Nonfullerene Acceptors, *InfoMat*, 2021, **3**(2), 175–200.
13 H. Gao, Y. Sun, L. Meng, C. Han, X. Wan and Y. Chen, Recent Progress in All-Small-Molecule Organic Solar Cells, *Small*, 2023, **19**(3), 2205594.
14 D. He, F. Zhao, C. Wang and Y. Lin, Non-Radiative Recombination Energy Losses in Non-Fullerene Organic Solar Cells, *Adv. Funct. Mater.*, 2022, **32**(19), 2111855.
15 P. Saeed, M. Adnan, Z. Irshad, R. Hussain, H. W. Darwish, M. Hussain, M. Ahmed and J. K. Lee, Molecular Engineering of Unidirectional Non-Fused Π-Bridge Containing Asymmetric Non-Fullerene Acceptors for High-Performance Organic Solar Cells, *Energy Technol.*, 2025, 2402465.
16 J. Hou, O. Inganäs, R. H. Friend and F. Gao, Organic Solar Cells Based on Non-Fullerene Acceptors, *Nat. Mater.*, 2018, **17**(2), 119–128.
17 Z. Luo, H. Yan and C. Yang, End-Group Engineering of Nonfullerene Acceptors for High-Efficiency Organic Solar Cells, *Acc. Mater. Res.*, 2023, **4**(11), 968–981.
18 Q. Shen, C. He, S. Li, L. Zuo, M. Shi and H. Chen, Design of Non-Fused Ring Acceptors toward High-Performance, Stable, and Low-Cost Organic Photovoltaics, *Acc. Mater. Res.*, 2022, **3**(6), 644–657.
19 B. He, L. Tang, X. Huang, J. Zhang, M. Xiao, G. Chen and C. Dai, Phthalimide-Based Unfused-Ring Non-Fullerene Acceptors for Constructing Efficient Organic Solar Cells with High Open-Circuit Voltage, *New J. Chem.*, 2024, **48**(3), 1272–1279.
20 J. M. Seminario, An Introduction to Density Functional Theory in Chemistry, *Theor. Comput. Chem.*, 1995, **2**(C), 1–27.
21 E. K. U. Gross and W. Kohn, Time-Dependent Density-Functional Theory, *Adv. Quantum Chem.*, 1990, **21**, 255–291.
22 Y. Cui, P. Zhu, X. Liao and Y. Chen, Recent Advances of Computational Chemistry in Organic Solar Cell Research, *J. Mater. Chem. C*, 2020, **8**(45), 15920–15939.
23 J. Tirado-Rives and W. L. Jorgensen, Performance of B3LYP Density Functional Methods for a Large Set of Organic Molecules, *J. Chem. Theory Comput.*, 2008, **4**(2), 297–306.
24 T. Yanai, D. P. Tew and N. C. Handy, A New Hybrid Exchange–Correlation Functional Using the Coulomb-Attenuating Method (CAM-B3LYP), *Chem. Phys. Lett.*, 2004, **393**(1–3), 51–57.
25 Y. Zhao, J. Pu, B. J. Lynch and D. G. Truhlar, Tests of Second-Generation and Third-Generation Density Functionals for Thermochemical Kinetics, *Phys. Chem. Chem. Phys.*, 2004, **6**(4), 673–676.
26 H. Fang and Y. Kim, Excited-State Tautomerization in the 7-Azaindole-$(H_2O)_n$ ($n = 1$ and 2) Complexes in the Gas Phase and in Solution: A Theoretical Study, *J. Chem. Theory Comput.*, 2011, **7**(3), 642–657.
27 J. E. Del Bene, W. B. Person and K. Szczepaniak, Properties of Hydrogen-Bonded Complexes Obtained from the B3LYP Functional with 6-31G(d,p) and 6-31+G(d, p) Basis Sets: Comparison with MP2/6-31+G(d, p) Results and Experimental Data, *J. Phys. Chem.*, 1995, **99**(27), 10705–10707.
28 N. M. O'boyle, A. L. Tenderholt and K. M. Langner, Cclib: A Library for Package-independent Computational Chemistry Algorithms, *J. Comput. Chem.*, 2008, **29**(5), 839–845.
29 J. J. Intemann, K. Yao, F. Ding, Y. Xu, X. Xin, X. Li and A. K. Y. Jen, Enhanced Performance of Organic Solar Cells with Increased End Group Dipole Moment in Indacenodithieno[3,2-b]Thiophene-Based Molecules, *Adv. Funct. Mater.*, 2015, **25**(30), 4889–4897.
30 S. Y. Leblebici, T. L. Chen, P. Olalde-Velasco, W. Yang and B. Ma, Reducing Exciton Binding Energy by Increasing Thin Film Permittivity: An Effective Approach To Enhance Exciton Separation Efficiency in Organic Solar Cells, *ACS Appl. Mater. Interfaces*, 2013, **5**(20), 10105–10110.
31 Y. Zhong, A. Tada, S. Izawa, K. Hashimoto and K. Tajima, Enhancement of V_{OC} without Loss of J_{SC} in Organic Solar Cells by Modification of Donor/Acceptor Interfaces, *Adv. Energy Mater.*, 2014, **4**(5), 1301332.
32 J. M. Randazzo, C. Marante, S. Chattopadhyay, B. I. Schneider, J. Olsen and L. Argenti, ASTRA: Transition-Density-Matrix Approach to Molecular Ionization, *Phys. Rev. Res.*, 2023, **5**(4), 043115.
33 T. Lu and F. Chen, Multiwfn: A Multifunctional Wavefunction Analyzer, *J. Comput. Chem.*, 2012, **33**(5), 580–592.
34 C.-P. Hsu, Reorganization Energies and Spectral Densities for Electron Transfer Problems in Charge Transport Materials, *Phys. Chem. Chem. Phys.*, 2020, **22**(38), 21630–21641.
35 V. Vehmanen, N. V. Tkachenko, H. Imahori, S. Fukuzumi and H. Lemmetyinen, Charge-Transfer Emission of Compact Porphyrin–Fullerene Dyad Analyzed by Marcus Theory of Electron-Transfer, *Spectrochim. Acta, Part A*, 2001, **57**(11), 2229–2244.
36 J. M. Mayer, Understanding Hydrogen Atom Transfer: From Bond Strengths to Marcus Theory, *Acc. Chem. Res.*, 2011, **44**(1), 36–46.

37 J. Wang, J. Zhu, C. Li, Y. Lin, X. Li, H. Zhang, Z. Ma and Y. Lu, Effect of Nitro-Substituted Ending Group on the Photovoltaic and Photocatalytic Performance of Non-Fullerene Acceptors, *Chem. Eng. J.*, 2024, **490**, 151467.

38 F. S. García Einschlag, J. Lopez, L. Carlos, A. L. Capparelli, A. M. Braun and E. Oliveros, Evaluation of the Efficiency of Photodegradation of Nitroaromatics Applying the UV/H_2O_2 Technique, *Environ. Sci. Technol.*, 2002, **36**(18), 3936–3944.

39 W. Guo, Y. Zheng, W. Xiang and Y. Zhang, Advances in the Catalysis of Reduction of Nitroaromatics and Its Mechanism: A Tutorial Review, *RSC Sustainability*, 2025, **3**(1), 243–254.

40 S. Zhou, X. Tao, Z. Liu, H. Wu, Z. Guan, L. Liu, J. Li, X. Chen and W. Ou-Yang, Regulation of Dihedral Angle on Molecular Engineering for Enhancing Triboelectric Performance, *Adv. Funct. Mater.*, 2024, **34**(40), 2405443.

41 K. Suzuki and H. Kaji, Torsion Angle Analysis of a Thermally Activated Delayed Fluorescence Emitter in an Amorphous State Using Dynamic Nuclear Polarization Enhanced Solid-State NMR, *J. Am. Chem. Soc.*, 2023, **145**(30), 16324–16329.

42 W. Humphrey, A. Dalke and K. Schulten, VMD: Visual Molecular Dynamics, *J. Mol. Graphics*, 1996, **14**(1), 33–38.

43 J. Lee, C. Sun, H. Jeon, T. H. Nguyen, T. N. Phan, X. Bao, Y. Kim and B. J. Kim, Efficient and Photostable Organic Solar Cells Achieved by Alloyed Dimer Acceptors with Tailored Linker Structures, *Adv. Funct. Mater.*, 2024, **34**(39), 2404569.

44 A. Mateo-Alonso, π-Conjugated Materials: Here, There, and Everywhere, *Chem. Mater.*, 2023, **35**(4), 1467–1469.

45 X. Bi, S. Li, T. He, H. Chen, Y. Li, X. Jia, X. Cao, Y. Guo, Y. Yang, W. Ma, *et al.*, Balancing Flexible Side Chains on 2D Conjugated Acceptors Enables High-Performance Organic Solar Cell, *Small*, 2024, **20**(24), 2311561.

46 H. Naz, M. Hussain, M. Adnan, R. Hussain, Z. Irshad, H. W. Darwish, U. Farooq, J. Yaqoob and J. Lim, Enhancing Optical and Optoelectronic Characteristics of Nonfused Ring-Containing Electron Acceptors for Efficient Organic Photovoltaics, *J. Phys. Chem. C*, 2025, **129**(26), 12204–12223.

47 S. Shi, S. Zhang, Z. Xue, X. Yao, G. Zhang, J. Gao, Y. Li, X. Tu, S. Zhang, C. Zhang, *et al.*, Near-Infrared Acceptors with Imide-Containing End Groups for Organic Solar Cells, *ACS Appl. Mater. Interfaces*, 2023, **15**(9), 12119–12126.

48 A. Ghaffar, M. Adnan, Z. Irshad, R. Hussain, A. Ghaffar, H. W. Darwish, F. Zafar and J. Lim, Structural Engineering of Small Molecule-Based Narrow Bandgap Dithieno-3,2-b:2′,3′-Dlpyrrole-Based Non-Fullerene Electron Acceptors for Efficient Organic Solar Cells, *Mater. Chem. Phys.*, 2025, **337**, 130611.

49 C.-Z. Yang, Z.-H. Pan, K. Zhang, J.-W. Tai, C.-K. Wang, L. Ding, M.-K. Fung and J. Fan, Intramolecular Charge Transfer Effect for Highly Efficient Deep Red and near Infrared Thermally Activated Delayed Fluorescence, *Mater. Horiz.*, 2023, **10**(3), 945–951.

50 Z. Xie, Z. Chen, H. Li, Q. Yan, H. Chen, X. Lin, I. Kaminer, O. D. Miller and Y. Yang, Maximal Quantum Interaction between Free Electrons and Photons, *Phys. Rev. Lett.*, 2025, **134**(4), 043803.

51 N. Shahzad, S. A. S. Chatha, R. Hussain, S. Hussain, J. Iqbal and M. Adnan, Impact of End-Capped Acceptor Modification in Anthanthrone-Based D-π-A Type Donor Materials for Organic and as Hole Transporting Materials for Perovskite Solar Cells, *J. Fluoresc.*, 2025, 1–26.

52 L. Ma, S. Zhang, J. Zhu, Z. Chen, T. Zhang, X. Hao and J. Hou, Design of Low-Cost Non-Fused Ultranarrow-Band-Gap Acceptors for Versatile Photovoltaic Applications, *Joule*, 2024, **8**(8), 2238–2249.

53 X. Cui, G. Ran, H. Lu, Y. Liu, H. Jiang, H. Zhang, D. Li, Y. Liu, Y. Lin, Z. Ma, *et al.*, Enabling Low Nonradiative Recombination Losses in Organic Solar Cells by Efficient Exciton Dissociation, *Adv. Funct. Mater.*, 2024, **34**(28), 2400219.

54 W. Liang, S. Zhu, K. Sun, J. Hai, Y. Cui, C. Gao, W. Li, Z. Wu, G. Zhang and H. Hu, Achieving 19.72% Efficiency in Ternary Organic Solar Cells through Electrostatic Potential-Driven Morphology Control, *Adv. Funct. Mater.*, 2025, **35**(7), 2415499.

55 P. Wang, F. Bi, Y. Li, C. Han, N. Zheng, S. Zhang, J. Wang, Y. Wu and X. Bao, Manipulating the Intermolecular Interactions through Side Chain Engineering and Unilateral Π-Bridge Strategy for Efficient Small Molecular Photovoltaic Acceptor, *Adv. Funct. Mater.*, 2022, **32**(23), 2200166.

56 B. Zhang, Y. Zhao, C. Xu, C. Feng, W. Li, X. Qin, M. Lv, X. Luo, X. Qin, A. Li, *et al.*, Perylene Diimide-Based Low-Cost and Thickness-Tolerant Electron Transport Layer Enables Polymer Solar Cells Approaching 19% Efficiency, *Adv. Funct. Mater.*, 2024, **34**(34), 2400903.

57 O. V. Mikhnenko, P. W. M. Blom and T.-Q. Nguyen, Exciton Diffusion in Organic Semiconductors, *Energy Environ. Sci.*, 2015, **8**(7), 1867–1888.

58 Q. Chen, Y. Gao, J. Dong, Y. Yang, H. Huang, F. Aniés, Z. Bian, X. Xu, C. Li, C. Yao, *et al.*, Alkoxy Modification of the Terminal Group in Nonfullerene Acceptors to Achieve Efficient Ternary Organic Solar Cells With a High Open-Circuit Voltage, *Adv. Funct. Mater.*, 2025, **35**(20), 2423287.

59 Y. Sun, L. Wang, C. Guo, J. Xiao, C. Liu, C. Chen, W. Xia, Z. Gan, J. Cheng, J. Zhou, *et al.*, π-Extended Nonfullerene Acceptor for Compressed Molecular Packing in Organic Solar Cells To Achieve over 20% Efficiency, *J. Am. Chem. Soc.*, 2024, **146**(17), 12011–12019.

60 Z. Han, K. Wang, Y. Chai, R. Zhang, J. Zhang, D. He, C. Wang and F. Zhao, Regulating the Miscibility of Donors/Acceptors to Manipulate the Morphology and Reduce Non-Radiative Recombination Energy Loss Enables Efficient Organic Solar Cells, *J. Mater. Chem. C*, 2024, **12**(11), 3873–3880.

61 J. Lee, C. Sun, B. S. Ma, H. J. Kim, C. Wang, J. M. Ryu, C. Lim, T. Kim, Y. Kim, S. Kwon, *et al.*, Efficient, Thermally Stable, and Mechanically Robust All-Polymer Solar Cells Consisting of the Same Benzodithiophene Unit-Based Polymer Acceptor and Donor with High Molecular Compatibility, *Adv. Energy Mater.*, 2021, **11**(5), 2003367.

62 Q. Fan, Q. An, Y. Lin, Y. Xia, Q. Li, M. Zhang, W. Su, W. Peng, C. Zhang, F. Liu, *et al.*, Over 14% Efficiency All-Polymer Solar Cells Enabled by a Low Bandgap Polymer Acceptor with Low Energy Loss and Efficient Charge Separation, *Energy Environ. Sci.*, 2020, **13**(12), 5017–5027.

63 Z. Wang, R. Meng, H. Guo, Y. Sun, Y. Liu, H. Zhang, Z. Cao, J. Dong, X. Xu, G. Liang, *et al.*, Toward High Efficient $Cu_2ZnSn(S_x,Se_{1-x})_4$ Solar Cells: Break the Limitations of V_{oc} and FF, *Small*, 2023, **19**(22), 2300634.

64 F. Xue, Y. Xie, Y. Cui, D. Yu Paraschuk, W. Ma and H. Yan, Boosting Fill Factor of Semitransparent Donor-Poor Organic Solar Cells for the Best Light Utilization Efficiency, *Adv. Funct. Mater.*, 2025, **35**(8), 2415617.

65 T. Huang, Z. Zhang, Q. Liao, D. Wang, Y. Zhang, S. Geng, H. Guan, Z. Cao, Y. Huang and J. Zhang, Achieved 18.9% Efficiency by Fine-Tuning Non-Fullerene Acceptor Content to Simultaneously Increase the Short-Circuit Current and Fill Factor of Organic Solar Cells, *Small*, 2023, **19**(47), 2303399.

66 J. Huang, H. Tang, C. Yan and G. Li, 1,1-Dicyanomethylene-3-Indanone End-Cap Engineering for Fused-Ring Electron Acceptor-Based High-Performance Organic Photovoltaics, *Cell Rep. Phys. Sci.*, 2021, **2**(1), 100292.

67 H. Zhuo, X. Li, J. Zhang, C. Zhu, H. He, K. Ding, J. Li, L. Meng, H. Ade and Y. Li, Precise Synthesis and Photovoltaic Properties of Giant Molecule Acceptors, *Nat. Commun.*, 2023, **14**(1), 7996.

68 D. Xie, T. Liu, W. Gao, C. Zhong, L. Huo, Z. Luo, K. Wu, W. Xiong, F. Liu, Y. Sun, *et al.*, A Novel Thiophene-Fused Ending Group Enabling an Excellent Small Molecule Acceptor for High-Performance Fullerene-Free Polymer Solar Cells with 11.8% Efficiency, *Sol. RRL*, 2017, **1**(6), 1700044.